Electronic Supplementary Information

Programmable Mismatches-fueled High-efficiency DNA Signal Amplifier

Xiao-Long Zhang[1], Sha-Sha Li[1], Wei-Wei Liu, Ling-Qi Kong, Ya-Qin Chai*, and Ruo Yuan*

†Key Laboratory of Luminescence Analysis and Molecular Sensing (Southwest University), Ministry of Education, College of Chemistry and Chemical Engineering, Southwest University, Chongqing 400715, PR China.

*Corresponding author. E-mail: yuanruo@swu.edu.cn; yqchai@swu.edu.cn

1 Authors Contribution: X. L. Zhang and S. S. Li contributed equally.

Table of content

Experimental Section

Chemical and Materials. Tris (2-carboxyethy) phosphine hydrochloride (TCEP), 6-Mercaptohexan-1-ol (MCH) and Gold chloride ($HAuCl_4 \bullet 4H_2O$) were obtained from Sigma (St. Louis, MO, USA). The oligonucleotides were provided by Tsingke (Beijing, China) and the specific sequences of the HPLC-purified oligonucleotides adopted in subsequent experiments were displayed in Table S1. Tris-HCl buffer (20 mM Tris, 1.0 mM $MgCl_2$, 140 mM NaCl, 5 mM KCl, 1.0 mM $CaCl_2$, 1.0 mM TCEP, pH 7.4) was harnessed as solvent to support the hybridization of oligonucleotides. 5 × TBE buffer (250 mM Tris, 250 mM H_3BO_3, 10 mM EDTA, pH 8.0), tetraethylenediamine (TEMED), ammonium persulfate (APS), acrylamide (29:1, 40%), and nucleic acid stain GelRed for polyacrylamide gel electrophoresis (PAGE) experiments were supplied by Dingguo Biotechnology Co., LTD (Chongqing, China). $[Fe(CN)_6]^{3-/4-}$ solution (20 mM Tris-HCl, 5 mM $K_4[Fe(CN)_6$, 5 mM $K_3[Fe(CN)_6]$,] pH 7.4) and Phosphate buffered solution (PBS) buffer (100 mM KH_2PO_4, 100 mM Na_2HPO_4, 100 mM KCl, pH 7.0) were used to study the electrochemical biosensing platform performance. Dulbecco's Modified Eagle Medium (DMEM), Lipofectamine Reagent-3000 and phosphate buffered saline (PBS) for cell experiments were purchased from Thermo Fisher Scientific Inc. (Shanghai, China).

Table S1. Synthetic Oligonucleotide Sequences

sequence	from 5' to 3'
DNA-182-5P	TTTGGCAATGGTAGAACTCACACT
2-H1-B	AGTGTG(a) AGTTCT(x) ACCATT(b) GCCAAA(y) TCCAAT(z*) CACAAC(c*) TTTGGC(y*) AATGGT(b*) AGAACT(x)
2-H1-B-M1C	AGTGTGAGTTCTACCATTGCCAAATCCAATCACAACTTTGGCAATG GTACAACT
2-H2-B-M2CC	AGTGTGAGTTCTACCATTGCCAAATCCAATCACAACTTTGGCAATG GTACCACT
2-H1-A	AGTGTGAGTTCTACCATTGCCAAATCCAATCACAACTTTGGCAATG GT
2-H2-B	ACCATT (b) GCCAAA(y) GTTGTG(c) ATTGGA(z) TTTGGC(y*) AATGGT(b*) TCCAAT(z*) CACAAC(c*) TTTGGC(y*)
2-H2-B-M1C	ACCATTGCCAAAGTTGTGATTGGATTTGGCAATGGT

2-H2-B-M2CC	TCCAATCACAACTCTGGC ACCATTGCCAAAGTTGTGATTGGATTTGGCAATGGT TCCAATCACAACTCCGGC
2-H2-A	ACCATTGCCAAAGTTGTGATTGGATTTGGCAATGGT TCCAATCACAAC
3-H1-B	AGTGTG(a) AGTTCT(x) ACCATT(b) GCCAAA(y) TCCAAT(z*) CACAAC(c*) TTTGGC(y*) AATGGT(b*) AGAACT(x*)
3-H1-B-M1C	AGTGTGAGTTCTACCATTGCCAAATCCAATCACAACTTTGGCAATG GTACAACT
3-H1-B-M2CC	AGTGTGAGTTCTACCATTGCCAAATCCAATCACAACTTTGGCAATG GTACCACT
3-H1-A	AGTGTGAGTTCTACCATTGCCAAATCCAATCACAACTTTGGCAATG GT
3-H2-B	ACCATT(b) GCCAAA(y) GTTGTG(c) ATTGGA(z) AGAACT(x*) CACACT(a*) TCCAAT(z*) CACAAC(c*) TTTGGC(y*)
3-H2-B-M1C	ACCATTGCCAAAGTTGTGATTGGAAGAACTCACACTTCCAATCACA ACTCTGGC
3-H2-B-M2CC	ACCATTGCCAAAGTTGTGATTGGAAGAACTCACACTTCCAATCACA ACTCCGGC
3-H2-A	ACCATTGCCAAAGTTGTGATTGGAAGAACTCACACTTCCAATCACA AC
3-H3-B	GTTGTG(c) ATTGGA(z) AGTGTG(a) AGTTCT(x) TTTGGC(y*) AATGGT(b*)AGAACT(x*) CACACT(a*) TCCAAT(z*)
3-H3-B-M1T	GTTGTGATTGGAAGTGTGAGTTCTTTTGGCAATGGTAGAACTCACA CTTTCAAT
3-H3-B-M2TA	GTTGTGATTGGAAGTGTGAGTTCTTTTGGCAATGGTAGAACTCACA CTTTAAAT
3-H3-A	GTTGTGATTGGAAGTGTGAGTTCTTTTGGCAATGGTAGAACTCACA CT
4-H1-B	AGTGTG(a) AGTTCT(x) ACCATT(b) GCCAAA(y) AACATC(w*) CACAAC(c*) TTTGGC(y*) AATGGT(b*) AGAACT(x*)
4-H1-B-M1C	AGTGTGAGTTCTACCATTGCCAAAAACATCCACAACTTTGGCAATG GTACAACT
4-H1-B-M2CC	AGTGTGAGTTCTACCATTGCCAAAAACATCCACAACTTTGGCAATG GTACCACT
4-H1-A	AGTGTGAGTTCTACCATTGCCAAAAACATCCACAACTTTGGCAATG GT
4-H2-B	ACCATT(b) GCCAAA(y) GTTGTG(c) GATGTT(w) TCCAAT(z*) CTACCG(d*) AACATC(w*) CACAAC(c*) TTTGGC(y*)
4-H2-B-M1C	ACCATTGCCAAAGTTGTGGATGTTTCCAATCTACCGAACATCCACA ACTCTGGC
4-H2-B-M2CC	ACCATTGCCAAAGTTGTGGATGTTTCCAATCTACCGAACATCCACA ACTCCGGC
4-H2-A	ACCATTGCCAAAGTTGTGGATGTTTCCAATCTACCGAACATCCACA AC
4-H3-B	GTTGTG(c) GATGTT(w) CGGTAG(d) ATTGGA(z) AGAACT(x*) CACACT(a*) TCCAAT(z*) CTACCG(d*) AACATC(w*)
4-H3-B-M1C	GTTGTGGATGTTCGGTAGATTGGAAGAACTCACACTTCCAATCTAC CGACCATC
4-H3-B-M2CA	GTTGTGGATGTTCGGTAGATTGGAAGAACTCACACTTCCAATCTAC CGACAATC
4-H3-A	GTTGTGGATGTTCGGTAGATTGGAAGAACTCACACTTCCAATCTAC CG

4-H4-B	CGGTAG(d) ATTGGA(z) AGTGTG(a) AGTTCT(x) TTTGGC(y*) AATGGT(b*) AGAACT(x*) CACACT(a*) TCCAAT(z*)
4-H4-B-M1T	CGGTAGATTGGAAGTGTGAGTTCTTTTGGCAATGGTAGAACTCACA CTTTCAAT
4-H4-B-M2TA	CGGTAGATTGGAAGTGTGAGTTCTTTTGGCAATGGTAGAACTCACA CTTTAAAT
4-H4-A	CGGTAGATTGGAAGTGTGAGTTCTTTTGGCAATGGTAGAACTCACA CT
2F-H2-B	BHQ1-ACCATTGCCAAAGTTGTGATTGGATTTGGCAATGGT TCCAATCACAACTTTGGC-FAM
2F-H2-B-M1C	BHQ1-ACCATTGCCAAAGTTGTGATTGGATTTGGCAATGGT TCCAATCACAACTCTGGC-FAM
2F-H2-B-M2CC	BHQ1-ACCATTGCCAAAGTTGTGATTGGATTTGGCAATGGT TCCAATCACAACTCCGGC-FAM
2F-H2-A	BHQ1-ACCATTGCCAAAGTTGTGATTGGATTTGGCAATGGT TCCAATCACAAC-FAM
3F-H3-B	BHQ1- GTTGTGATTGGAAGTGTGAGTTCTTTTGGCAATGGTAGAACTCACA CTTCCAAT-FAM
3F-H3-B-M1T	BHQ1- GTTGTGATTGGAAGTGTGAGTTCTTTTGGCAATGGTAGAACTCACA CTTTCAAT-FAM
3F-H3-B-M2TA	BHQ1- GTTGTGATTGGAAGTGTGAGTTCTTTTGGCAATGGTAGAACTCACA CTTTAAAT-FAM
3F-H3-A	BHQ1- GTTGTGATTGGAAGTGTGAGTTCTTTTGGCAATGGTAGAACTCACA CT-FAM
4F-H4-B	BHQ1- CGGTAGATTGGAAGTGTGAGTTCTTTTGGCAATGGTAGAACTCACA CTTCCAAT-FAM
4F-H4-B-M1T	BHQ1- CGGTAGATTGGAAGTGTGAGTTCTTTTGGCAATGGTAGAACTCACA CTTTCAAT-FAM
4F-H4-B-M2TA	BHQ1- CGGTAGATTGGAAGTGTGAGTTCTTTTGGCAATGGTAGAACTCACA CTTTAAAT-FAM
4F-H4-A	BHQ1- CGGTAGATTGGAAGTGTGAGTTCTTTTGGCAATGGTAGAACTCACA CT-FAM
2E-H1-B	AGTGTGAGTTCTACCATTGCCAAATCCAATCACAACTTTGGCAATG GTAGAACT-Fc
2E-H2-B	SH-TTTTTTACCATTGCCAAAGTTGTGATTGGATTTGGCAATGGT TCCAATCACAACTTTGGC
2E-H1-B-M2CC	AGTGTGAGTTCTACCATTGCCAAATCCAATCACAACTTTGGCAATG GTACCACT-Fc
2E-H2-B-M2CC	SH-TTTTTTACCATTGCCAAAGTTGTGATTGGATTTGGCAATGGT TCCAATCACAACTCCGGC
3E-H1-B	AGTGTGAGTTCTACCATTGCCAAATCCAATCACAACTTTGGCAATG GTAGAACT-Fc
3E-H2-B	ACCATTGCCAAAGTTGTGATTGGAAGAACTCACACTTCCAATCACA ACTTTGGC-Fc
3E-H3-B	SH-

	TTTTTTGTTGTGATTGGAAGTGTGAGTTCTTTTGGCAATGGTAGAAC TCACACTTCCAAT
3E-H1-B-M2CC	AGTGTGAGTTCTACCATTGCCAAATCCAATCACAACTTTGGCAATG GTACCACT-Fc
3E-H2-B-M2CC	ACCATTGCCAAAGTTGTGATTGGAAGAACTCACACTTCCAATCACA ACTCCGGC-Fc
	SH-
3E-H3-B-M2TA	TTTTTTGTTGTGATTGGAAGTGTGAGTTCTTTTGGCAATGGTAGAAC TCACACTTTAAAT
4E-H1-B	AGTGTGAGTTCTACCATTGCCAAAAACATCCACAACTTTGGCAATG GTAGAACT-Fc
4E-H2-B	ACCATTGCCAAAGTTGTGGATGTTTCCAATCTACCGAACATCCACA ACTTTGGC-Fc
4E-H3-B	GTTGTGGATGTTCGGTAGATTGGAAGAACTCACACTTCCAATCTAC CGAACATC-Fc
	SH-
4E-H4-B	TTTTTTCGGTAGATTGGAAGTGTGAGTTCTTTTGGCAATGGTAGAA CTCACACTTCCAAT
4E-H1-B-M2CC	AGTGTGAGTTCTACCATTGCCAAAAACATCCACAACTTTGGCAATG GTACCACT-Fc
4E-H2-B-M2CC	ACCATTGCCAAAGTTGTGGATGTTTCCAATCTACCGAACATCCACA ACTCCGGC-Fc
4E-H3-B-M2CA	GTTGTGGATGTTCGGTAGATTGGAAGAACTCACACTTCCAATCTAC CGACAATC-Fc
	SH-
4E-H4-B-M2TA	TTTTTTCGGTAGATTGGAAGTGTGAGTTCTTTTGGCAATGGTAGAA CTCACACTTTAAAT
FISH-FAM	FAM-AGTGTGAGTTCTACCATTGCCAAA
FISH-BHQ1	GGTAGAACTCACACT-BHQ1
miRNA-182-5p	UUU GGC AAU GGU AGA ACU CAC ACU
miRNA-21	UAGCUUAUCAGACUGAUGUUGA
miRNA-141	UAACACUGUCUGGUAAAGAUGG
miRNA-155	UUAAUGCUAAUCGUG AUAGGGGU

Apparatus and Measurements. Electrochemical Impedance Spectroscopy (EIS), Square Wave Voltammetry (SWV), and Cyclic Voltammetry (CV) were accomplished with a three-electrode arrangement via the electrochemical workstation (CHI760E, CH Instruments, Shanghai, China). Ultraviolet-visible (UV-vis) spectra was conducted by a UV-2501 PC Spectrometer (Shimadzu, Japan) and the fluorescence experiments were carried out by a SpectraMax Synergy H1 microplate reader (BioTek, USA). Fluorescence miRNA imaging in living cancer cells was carried out by a Total Internal Reflection Fluorescence (TIRF) microscopy (Olympus IX-81 microscope, Japan). The morphology characterization was investigated by an atomic force microscope (AFM, Bruker, Germany). The PAGE experiments were performed by the Bio-Rad

imaging system (Hercules, CA, USA). The CV and EIS response of the biosensing platform development were performed with the potential from -0.2 V to 0.6 V in $[Fe(CN)_6]^{3-/4-}$ solution (5 mM) with a scan rate of 100 $mV \cdot s^{-1}$). And the SWV was conducted in PBS (0.1 M) with the potential from 0.2 V to 0.7 V (Amplitude 25mV, Frequency 15 Hz, and Quiet time 2 s), which was applied to assess the performance of the developed electrochemical biosensor under the optimal experimental conditions.

Preparation Process of the Hairpin DNAs. The DNA strands (H1, H2, H3, and H4) were diluted in Tris-Hcl buffer (pH=7.4) and kept at 95 ^oC for 10 min, respectively, and then cooled down to 25 ^oC (30 min) to generate the hairpin DNAs. The prepared hairpin DNAs were adopted in next experiments.

Assembly of the Developed Biosensor. At first, the bare electrode (GCE, 4 mm in diameter) was cleaned with alumina slurry (0.3 μm and 0.05 μm) and treated by ultrasonic with ethanol and distilled water, respectively. Next, the electrode was electrodeposited with a layer of gold nanoparticles (depAu) in $HAuCl_4$ aqueous solution (1%) (-0.2 V, 30 s).

After that, 10 μL solution of the sulfhydryl labeled hairpin DNA was incubated on the modified electrode surface (depAu/GCE) overnight (25 ^oC). Then, the electrode was cleaned by Tris-HCl buffer, remaining active sites of electrode were blocked by the MCH (5 mM, 10 min), following by the cleaning treatment with ethanol and distilled water for three times.

Catalytic Multiple-arm DNA Junction Assembly (CMDJA) on the Electrode. Firstly, the prepared ferrocene labeled hairpin DNAs were mixed with different concentrations of target (Tris-HCl buffer) and dripped on the electrode (MCH/hairpin DNA/depAu/GCE) to react under the optimal experimental conditions.

Cell Culture and Total RNA Extraction. The cancer cells (HeLa and MCF-7) adopted here

were purchased by the cell bank of the Chinese Academy of Sciences (Shanghai, China). According to the corresponding protocols, these cells were cultivated in DMEM medium (10% fetal calf serum (FCS), 100 $U \cdot mL^{-1}$ penicillin, 100 $\mu g \cdot mL^{-1}$ streptomycin, Thermo Scientific Hyclone, USA) at 37 °C in 5% CO_2 incubator. Next, the total RNA samples were extracted from these cells by using the Trizol Reagent (Invitrogen Biotechnology Co., Ltd.) based on the operating protocols. Finally, the obtained cellular extracts were stored at -80 °C for subsequent experiments.

MiRNAs Imaging in Living Cells based on TIRF Microscopy. The processes for miRNA imaging in living cancer cells based TIRF microscopy were displayed as follows. At first, the HeLa, 22RV1, and A549 cells were transferred into a 35 mm^2 Petri dish. Then, the cells were cultivated in DMEM medium (5% CO_2, 37 °C, 24 h), respectively, to obtain 80% cell anchorage-dependent rate, following by the washing treatment via sterile PBS. Subsequently, the 50 μL containing Lipofectamine Reagent and hairpin DNA substrates was incubated into HeLa cells Petri dish, 22RV1 cells Petri dish, and A549 cells Petri dish, separately. Next, the cells were stained by the Hoechst 33342 solution (12 min) and cleaned for three times with PBS. Finally, the cells were incubated with freshly-prepared (1 mL) DMEM medium at 25 °C before miRNA imaging via fluorescence.

Polyacrylamide-Gel Electrophoresis (PAGE). Firstly, acrylamide (40%, 5 mL), distilled water (15 mL), 5xTBE buffer (5 mL), APS (5%, 200 μL), and TEMED (15 μL) were added successively with constant stirring for 1 min, the mixture above was transferred into the mould and stained for 10 min under 25 °C for ultimate formation of polyacrylamide gel (8%). After the DNA-loading buffer were added into the DNA samples (volume ratio 1:5), the dynamic products of DNA assembly were investigated by PAGE experiments on a fresh 8% polyacrylamide gel in

1× TBE buffer at 50 mA.

Biosensor Operation for the MiRNA-182-5P Detection in Cancer Cell Lysates. First, the prepared DNA substrates were mixed with the cancer cell lysates from different number of cells in Tris-HCl buffer (pH 7.4), next, 10 μL of the mixture above was incubated on the modified electrode surface under optimal experimental conditions. At last, the reacted electrode was cleaned with Tris-HCl buffer (pH 7.4) for next experiments.

Characterization of the CMDJA

Firstly, the reaction mechanism of catalytic multiple-arm DNA junction assembly (CMDJA) was characterized by PAGE. As the results of two-arm DNA junction shown in Fig. S1A, the obvious bands in lanes 1-3 correspond to miRNA-182-5P, 2-H1, and 2-H2 separately. After the miRNA-182-5P reacted with 2-H1, compared with lane 1 and lane 2, we can notice an obvious band with much slower migration (duplex 2-H1-miRNA-182-5p) and the band representing miRNA-182-5P vanished (lane 4), indicating that the 2-H1 has hybridized with the target miRNA-182-5P. Then, after the 2-H2 was mixed with the solution of 2-H1 and miRNA-182-5P, another bright band with slow migration (lane 5) compared with that of duplex 2-H1-miRNA-182-5P, which represented to the duplex H1-H2 (two-arm) was observed, suggesting that the 2-H2 has reacted with duplex 2-H1-miRNA-182-5P and displaced the miRNA-182-5P comparing with lane 4. Similarly, the self-assembly of three-arm DNA junction and four-arm DNA junction were also verified in the Fig. S1B (lane 7) and Fig. S1C (lane 9) respectively. These observations strongly indicated that these CMDJAs could be successfully proceeded.

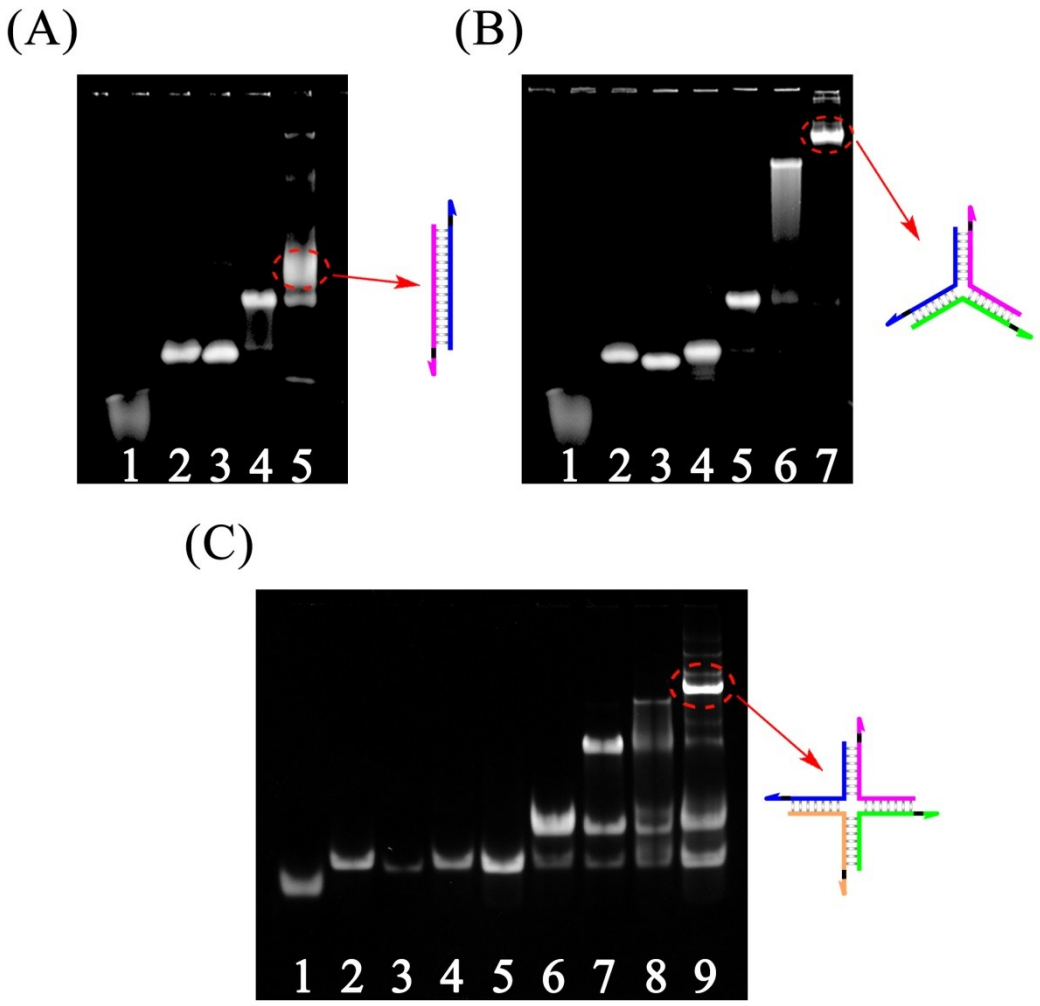

Fig. S1. Nondenaturing PAGE characterization of self-assembly of (A) two-arm DNA junction: lane 1, miRNA-182-5P (4 μM); lane 2, 2-H1 (1 μM); lane 3, 2-H2 (1 μM); lane 4, microRNA-182-5P (1 μM) and 2-H1 (1 μM); lane 5, microRNA-182-5P (1 μM), 2-H1 (1 μM), and 2-H2 (1 μM); (B) three-arm DNA junction: lane 1, miRNA-182-5P (4 μM); lane 2, 3-H1 (1 μM); lane 3, 3-H2 (1 μM); lane 4, 3-H3 (1 μM); lane 5, microRNA-182-5P (1 μM) and 3-H1 (1 μM); lane 6, microRNA-182-5P (1 μM), 3-H1 (1 μM), and 3-H2 (1 μM); lane 7, miRNA-182-5P (1 μM), 3-H1 (1 μM), 3-H2 (1 μM), and 3-H3 (1 μM); (C) four-arm DNA junction: lane 1, miRNA-182-5P (4 μM); lane 2, 4-H1 (1 μM); lane 3, 4-H2 (1 μM); lane 4, 4-H3 (1 μM); lane 5, 4-H4 (1 μM); lane 6, microRNA-182-5P (1 μM) and 4-H1 (1 μM); lane 7, microRNA-182-5P (1 μM), 4-H1 (1 μM), and 4-H2 (1 μM); lane 8, miRNA-182-5P (1 μM), 4-H1 (1 μM), 4-H2 (1 μM), and 4-H3 (1 μM); lane 9, miRNA-182-5P (1 μM), 4-H1 (1 μM), 4-H2 (1 μM), 4-H3 (1 μM), and 4-H4 (1 μM) (PAGE 8%,50 mA, 30

min).

AFM Characterization of the CMDJA

We further employed the atomic force microscope (AFM) to further verify the formation of the DNA junctions of three-arm and four-arm. As the shown in Fig. S2, the results corresponding morphologies and diameters showed relatively obvious three branches (Fig. S2A) and four branches (Fig. S2C), verifying the successful assembly of these CMDJA.

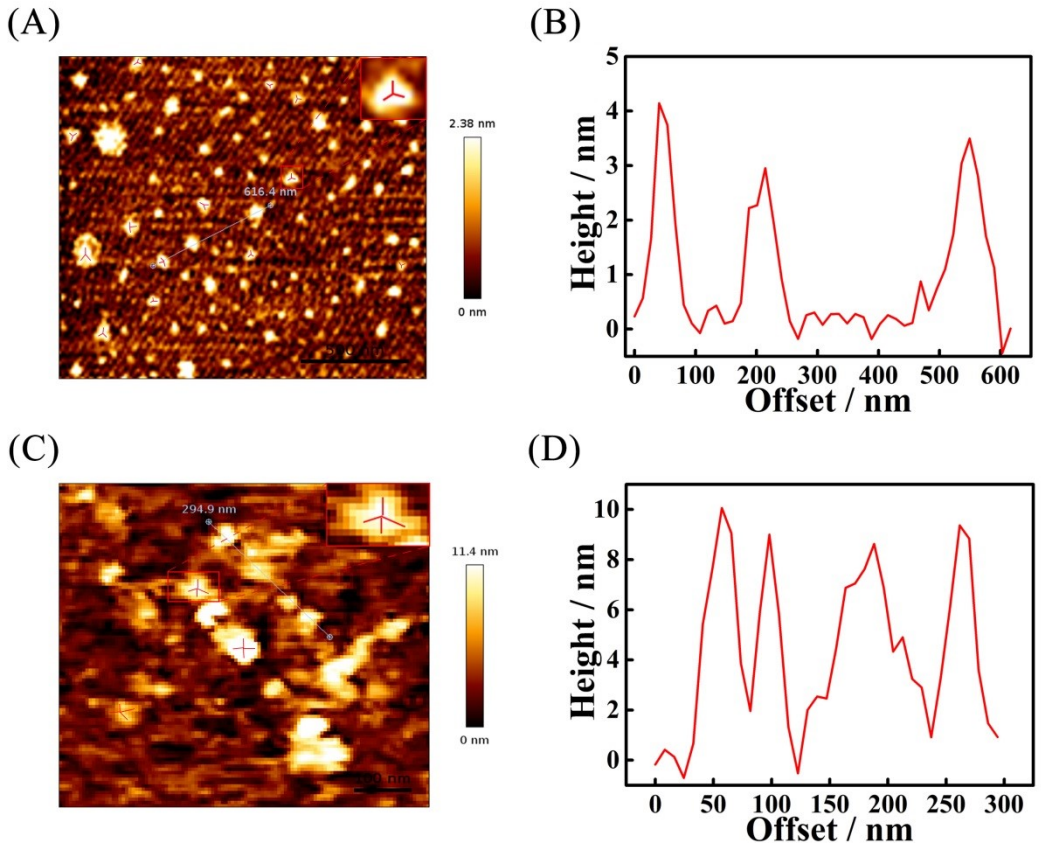

Fig. S2. (A)AFM images of the three-arm DNA junction and (B) corresponding height of sample on the diagonal. (C) AFM images of the four-arm DNA junction and (B) corresponding height of sample on the diagonal.

Electrochemical Characterization of the Proposed Biosensing Platform based on M-CFDJA

The CV and EIS were used to verify the stepwise fabrication of the biosensing platform

based on M-CFDJA. As displayed in Fig. S3A (CV), a pair of well-defined redox peaks (curve a) of the bare GCE could be noticed. When the GCE was electrodeposited with the AuNPs, the corresponding currents response increased (curve b), for the outstanding conductivity (AuNPs). Subsequently, with the immobilization of hairpin 4-H4, the current response dramatically decreased (curve c), because of the repulsion effect of negatively charge of the DNA and $[Fe(CN)_6]^{3-/4-}$. And when the MCH was self-assembly on the electrode surface, the current response decreased slightly (curve d), further meaning that the electrode surface almost has been occupied with the 4-H4.

Then as depicted in Fig. S3B (EIS), a small semicircle diameter and a long tail denoting diffusion could be observed, for the good conductivity of the bare GCE (curve a). And we can find a nearly straight line after the depAu was modified onto the electrode surface (curve b), because of the large surface area and the outstanding conductivity of the depAu. Next, with the self-assembly of more DNA strands and MCH onto the modified electrode surface, a dramatically increasing trend of R_{et} (curves c, d) could be noticed due to the improved steric hindrance of the DNA strands and MCH. These EIS results were consistent to the CV results which were observed above, further demonstrating the successful fabrication of this biosensor.

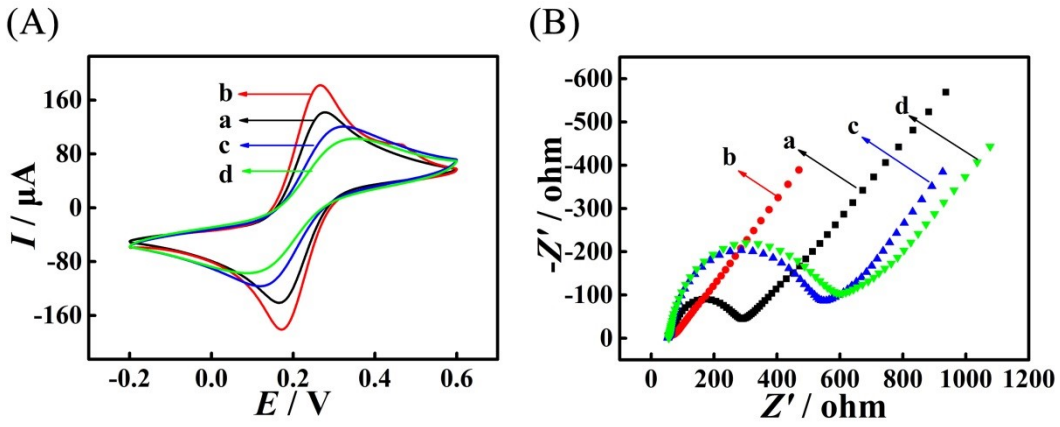

Fig. S3. (A) Typical CV and (B) EIS responses of electrodes modified with different components: (a) bare

GCE, (b) depAu/GCE, (c) 4-H4/depAu-GCE, (d) MCH/4-H4/depAu/GCE.

Moreover, the electroactive area of the modified electrode (depAu/GCE) and the immobilization density of H3 modified on the electrode surface were also determined by CV and chronocoulometry (CC). Firstly, CV studies were carried out according to the previous works.[1,2] The cyclic voltammograms (CVs) were operated[3] in 5 mM $[Fe(CN)_6]^{3-/4-}$ solution with different potential scan rates (10, 30, 50, 70, 90, 110, 130, 150, 170, 190, and 210 mV/s), as depicted in following Fig. S4A. The linear relationship for the current response (I_p) versus the square root of scan rate ($v^{1/2}$) is presented in following Fig. S4B. On the basis of the Randles-Sevcik equation:

$$I_p = (2.69\times10^5)n^{3/2}AD^{1/2}cv^{1/2} \qquad (4)$$

the electroactive area A can be expressed as eqn (2).

$$A = S/(2.69\times10^5)n^{3/2}D^{1/2}c \qquad (5)$$

(S: the slope, n: number of electrons involved (n=1), D: diffusion coefficient (6.72×10^{-6} cm^2 s^{-1}, 25 ℃), c: ferricyanide concentration (5 mM)). Thus the electroactive area A of the electrode surface (depAu/GCE) was computed as 16.9 mm^2.

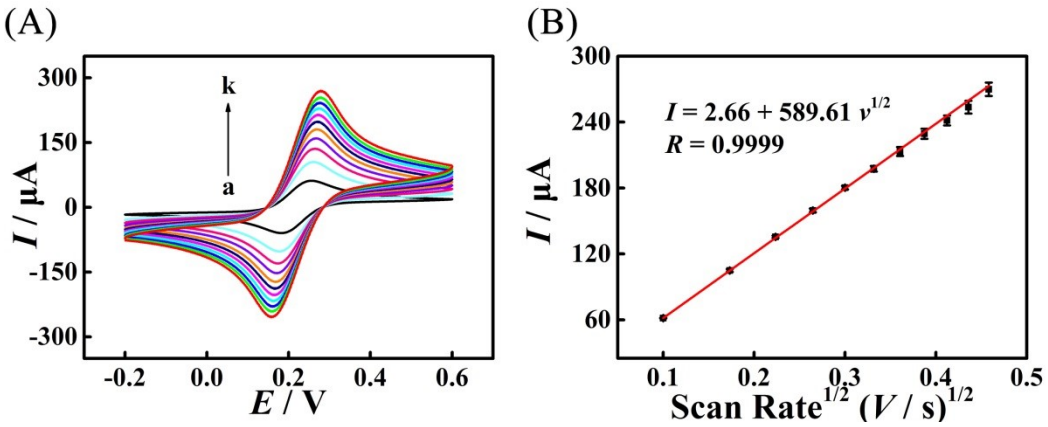

Fig. S4. (A) CVs of electrode (depAu/GCE) in 5.0 mM $Fe(CN)_6^{3-/4-}$ at different scan rates (a-k: 10, 30, 50, 70, 90, 110, 130, 150, 170, 190, and 210 mV/s); (B) Calibration curve for Ip *vs* $v^{1/2}$ (Error bars, SD, n = 3).

Secondly, according to the previous report,[4] the CC studies were performed and the density of H3 Γss was computed based on the following eqn (6) and (7).

$$\Gamma_{ss} = (Q_{ss}N_A/nFA)(z/m) \qquad (6)$$

$$Q_{ss} = Q_{total} - Q_{dl} \qquad (7)$$

(N_A: Avogadro's number, n: electrons number, A: electroactive area, m: number of nucleotides in the DNA, z: charge of the redox molecule). Q_{total} and Q_{dl} are obtained from the plot of the charge (Q) versus the square root of scan time ($t^{1/2}$), as shown in following Fig.S5. The density of 4-H4 on the modified electrode (depAu/GCE) is therefore calculated as 6.32×10^{11} molecules·cm^{-2}.

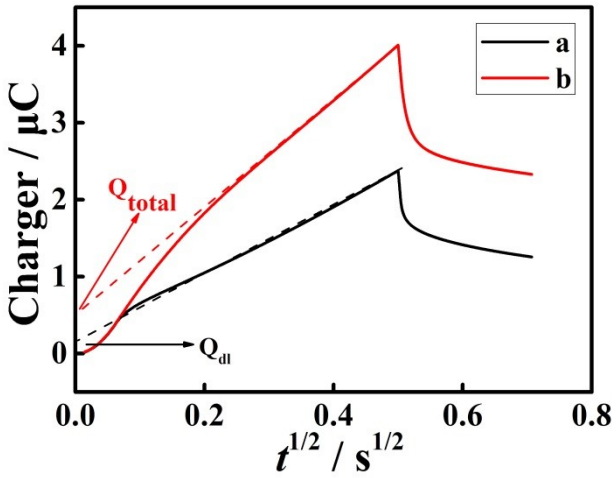

Fig. S5. Chronocoulometric curves of depAu/GCE modified with H3 (2 μM) (a) in 10 mM Tris-HCl (pH 7.4) and (b) in 10 mM Tris-HCl (pH 7.4) containing 50 μM RuHex.

Thermodynamic Parameters of CMDJA and M-CMDJA

Table S2. Thermodynamic Parameters of CMDJA and M-CMDJA (T = 25 °C)

Sequence	From 5' to 3'	ΔG_1 (kcal.mol^{-1})
2-H1-B	AGTGTGAGTTCTACCATTGCCAAATCCAATCACAACTTTGGCA ATGGTAGAACT	-23.51
2-H1-B-M1	AGTGTGAGTTCTACCATTGCCAAATCCAATCACAACTTTGGCA ATGGTACAACT	-17.89
2-H1-B-M2	AGTGTGAGTTCTACCATTGCCAAATCCAATCACAACTTTGGCA ATGGTACCACT	-16.99
2-H1-A	AGTGTGAGTTCTACCATTGCCAAATCCAATCACAACTTTGGCA ATGGT	-15.38
2-H2-B	ACCATTGCCAAAGTTGTGATTGGATTTGGCAATGGT TCCAATCACAACTTTGGC	-24.79
2-H2-B-M1	ACCATTGCCAAAGTTGTGATTGGATTTGGCAATGGT	-19.74

	TCCAATCACAACTCTGGC	
2-H2-B-M2	ACCATTGCCAAAGTTGTGATTGGATTTGGCAATGGT TCCAATCACAACTCCGGC	-18.93
2-H2-A	ACCATTGCCAAAGTTGTGATTGGATTTGGCAATGGT TCCAATCACAAC	-14.88
2-arm-B	-	-61.12
2-arm-B-M1	-	-61.12
2-arm-B-M2	-	-61.12
2-arm-A	-	-60.73
3-H1-B	AGTGTGAGTTCTACCATTGCCAAATCCAATCACAACTTTGGCA ATGGTAGAACT	-23.51
3-H1-B-M1	AGTGTGAGTTCTACCATTGCCAAATCCAATCACAACTTTGGCA ATGGTACAACT	-17.89
3-H1-B-M2	AGTGTGAGTTCTACCATTGCCAAATCCAATCACAACTTTGGCA ATGGTACCACT	-16.99
3-H1-A	AGTGTGAGTTCTACCATTGCCAAATCCAATCACAACTTTGGCA ATGGT	-15.38
3-H2-B	ACCATTGCCAAAGTTGTGATTGGAAGAACTCACACTTCCAATC ACAACTTTGGC	-28.49
3-H2-B-M1	ACCATTGCCAAAGTTGTGATTGGAAGAACTCACACTTCCAATC ACAACTCTGGC	-23.45
3-H2-B-M2	ACCATTGCCAAAGTTGTGATTGGAAGAACTCACACTTCCAATC ACAACTCCGGC	-22.64
3-H2-A	ACCATTGCCAAAGTTGTGATTGGAAGAACTCACACTTCCAATC ACAAC	-18.02
3-H3-B	GTTGTGATTGGAAGTGTGAGTTCTTTTGGCAATGGTAGAACTC ACACTTCCAAT	-23.16
3-H3-B-M1	GTTGTGATTGGAAGTGTGAGTTCTTTTGGCAATGGTAGAACTC ACACTTTCAAT	-19.03
3-H3-B-M2	GTTGTGATTGGAAGTGTGAGTTCTTTTGGCAATGGTAGAACTC ACACTTTAAAT	-15.81
3-H3-A	GTTGTGATTGGAAGTGTGAGTTCTTTTGGCAATGGTAGAACTC ACACT	-13.97
3-arm-B	-	-107.44
3-arm-B-M1	-	-107.44
3-arm-B-M2	-	-107.44
3-arm-A	-	-106.18
4-H1-B	AGTGTGAGTTCTACCATTGCCAAAAACATCCACAACTTTGGCA ATGGTAGAACT	-23.44
4-H1-B-M1	AGTGTGAGTTCTACCATTGCCAAAAACATCCACAACTTTGGCA ATGGTACAACT	-17.82
4-H1-B-M2	AGTGTGAGTTCTACCATTGCCAAAAACATCCACAACTTTGGCA ATGGTACCACT	-16.92
4-H1-A	AGTGTGAGTTCTACCATTGCCAAAAACATCCACAACTTTGGCA ATGGT	-15.31
4-H2-B	ACCATTGCCAAAGTTGTGGATGTTTCCAATCTACCGAACATCC ACAACTTTGGC	-25.17
4-H2-B-M1	ACCATTGCCAAAGTTGTGGATGTTTCCAATCTACCGAACATCC ACAACTCTGGC	-20.13
4-H2-B-M2	ACCATTGCCAAAGTTGTGGATGTTTCCAATCTACCGAACATCC ACAACTCCGGC	-19.32
4-H2-A	ACCATTGCCAAAGTTGTGGATGTTTCCAATCTACCGAACATCC ACAAC	-14.7

4-H3-B	GTTGTGGATGTTCGGTAGATTGGAAGAACTCACACTTCCAATC TACCGAACATC	-27.48
4-H3-B-M1	GTTGTGGATGTTCGGTAGATTGGAAGAACTCACACTTCCAATC TACCGACCATC	-22.72
4-H3-B-M2	GTTGTGGATGTTCGGTAGATTGGAAGAACTCACACTTCCAATC TACCGACAATC	-20.92
4-H3-A	GTTGTGGATGTTCGGTAGATTGGAAGAACTCACACTTCCAATC TACCG	-18.55
4-H4-B	CGGTAGATTGGAAGTGTGAGTTCTTTTGGCAATGGTAGAACTC ACACTTCCAAT	-23.16
4-H4-B-M1	CGGTAGATTGGAAGTGTGAGTTCTTTTGGCAATGGTAGAACTC ACACTTTCAAT	-19.03
4-H4-B-M2	CGGTAGATTGGAAGTGTGAGTTCTTTTGGCAATGGTAGAACTC ACACTTTAAAT	-15.81
4-H4-A	CGGTAGATTGGAAGTGTGAGTTCTTTTGGCAATGGTAGAACTC ACACT	-13.97
4-arm-B	-	-146.37
4-arm-B-M1	-	-146.37
4-arm-B-M2	-	-146.37
4-arm-A	-	-144.15

Comparison of the Δ*G* between the different M-CMDJA and CMDJA systems

Table S3. Comparison of the Δ*G* between the different M-CMDJA and CMDJA systems (T = 25 °C)

M-CMDJA and CMDJA	B / (kcal·mol^{-1})	B-M1 / (kcal·mol^{-1})	B-M2 / (kcal·mol^{-1})
Two-arm	-12.82	-23.49	-25.2
Three-arm	-32.28	-47.07	-52
Four-arm	-47.12	-66.67	-73.4

Background Leakage of the CMDJA and M-CMDJA

To study the background leakage of these CMDJA and M-CMDJA, PAGE experiments were performed to verify the yield of multiple-arm DNA junction by self-assembly without miRNA. As the results shown Fig. S6, the background leakage of two-arm (Fig. S6A), three-arm (Fig. S6B), and four-arm (Fig. S6C) with low free-energy landscapes (Scheme. 2, group A) resulted high background leakage (lane 1), which hindered the further application in improving the sensitivity and accuracy for the biomarkers assay. In the wild CMDJA (Scheme. 2, group B), since the pretty high free-energy landscapes, the corresponding background leakage was unobvious (lane 2). Moreover, when the mismatches was introduced in hairpin DNA substrates

with relatively suitable free-energy landscapes, the M-CMDJA (Scheme. 2, group B-M1 and group B-M2) showed almost ignorable background leakage (lane 3 and lane 4) compared with lane 1, certifying the excellent application prospect of these M-CMDJA in DNA nanotechnology, biomarker assay, and other areas.

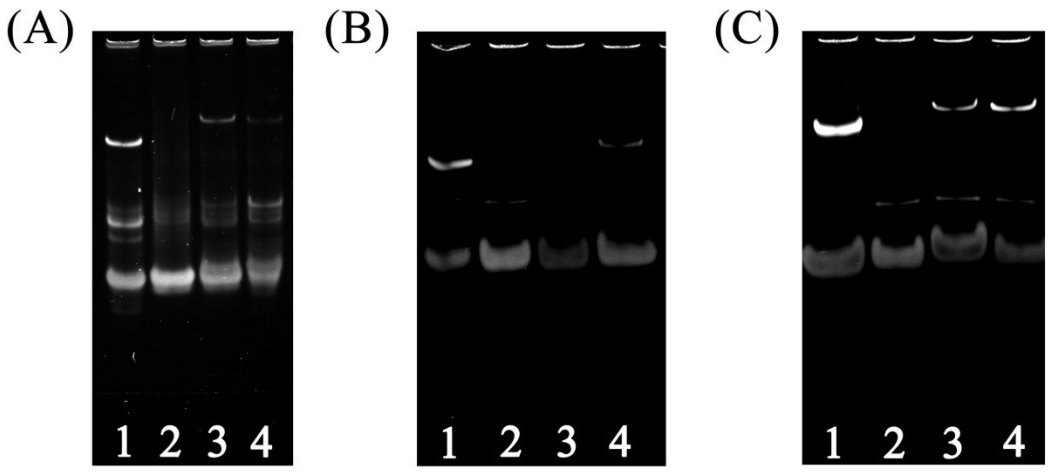

Fig. S6. Nondenaturing PAGE characterization of the background leakage of (A) two-arm DNA junction, (B) three-arm DNA junction, and (C) four-arm DNA junction by self-assembly without target miRNA-182-5P (lane 1, group A; lane 2, group B; lane 3, group B-M1; lane 4, group B-M2).

Fluorescence Response of Fluorescence Group with Different Concentration

To measure the practical conversion efficiency *N* of CMDJA in fluorescence, we firstly explored the relationship between the fluorescence response and the concentration of the fluorescent tag FAM labeled on the substrate DNA. As exhibited in Fig. S7A, as the increased concentration of FAM, the fluorescence intensity increased obviously and illustrated a well liner relationship with the FAM concentration. And the related regression equation was $Fi = 200.66 + 23494.78\ c$ (from 0.05 μM to 1.1 μM, R=0.9959).

Subsequently, we calculated the accurate conversion efficiency of different multiple-arms system.

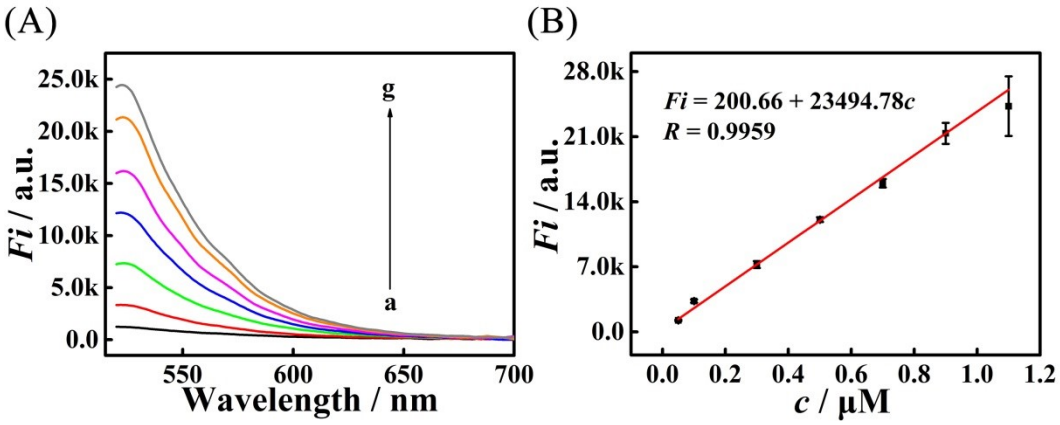

Fig. S7. (A) Fluorescence intensity of the FAM with different concentrations: (a) 0.05 μM, (b) 0.1 μM, (c) 0.3 μM, (d) 0.5 μM, (e) 0.7 μM, (f) 0.9 μM, (g) 1.1 μM and (B) corresponding calibration plot of the fluorescence intensity *vs* *c* (error bars, SD, *n* = 3; EX WL: 492 nm, EM WL: 520-700 nm, Gain: 75)

Electrochemical Response of the Biosensing Platform Immobilized with Different Multiple-arm DNA Junctions

To compare the feasibility of the M-CMDJA, the relationship of the electrochemical signal peak value of biosensor to multiple-arm DNA junction with different concentrations was performed using the SWV. As depicted in Fig. S8, the biosensor was incubated with two-arm DNA junction (Fig. S8A), three-arm DNA junction (Fig. S8D), and four-arm DNA junction (Fig. S8G) with different concentrations, respectively, which can be directly immobilized on the modified electrode (depAu/GCE) through Au-S bond to generate an significant variation of electrochemical signal. As shown in Fig. S8, with the concentration of multiple-arm DNS changed from 0 μM to 1.1 μM, the SWV signal value increased and depicted a well linear relationship with the corresponding concentration (two-arm DNA junction, Fig. S8B; three-arm DNA junction, Fig. S8E; four-arm DNA junction, Fig. S8H). The corresponding regression equation was $I = 0.2329 + 1.5858c$ ($R = 0.9956$, Fig. S8C), $I = 0.2503 + 1.8471c$ ($R = 0.9956$, Fig. S8F), and $I = 0.2530 + 2.5554c$ ($R = 0.9987$, Fig. S8I) respectively (I: electrochemical signal value, c: concentration of independent multiple-arm DNA junction; unit of c was μM). It can be concluded that the biosensing platform showed the most sensitive response to the four-arm DNA junction, demonstrating the superiority of four-arm DNA junction in electrochemical biosensor construction.

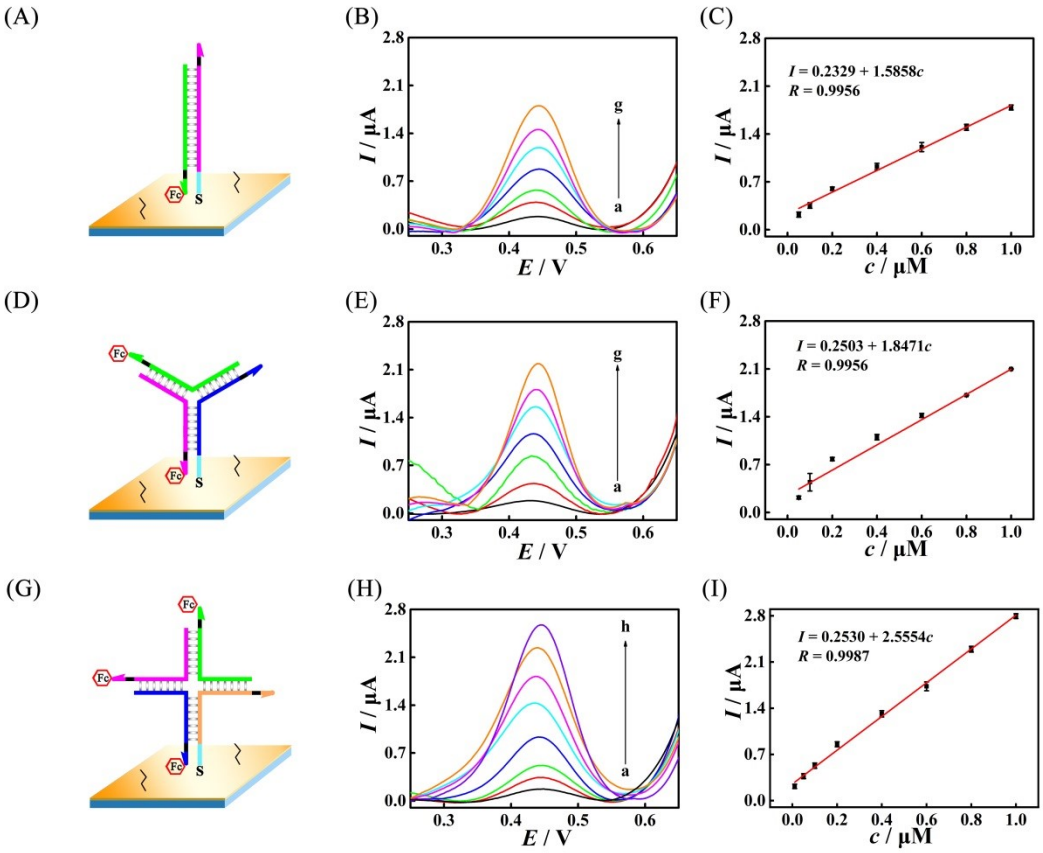

Fig. S8. Schematic illustration of biosensing platform immobilized with (A) two-arm DNA junction, (D) three-arm DNA junction, and (G) four-arm DNA junction. SWV peak value of the biosensor to (B) two-arm DNA junction: (a) 0.05 μM, (b) 0.1 μM, (c) 0.2 μM, (d) 0.4 μM, (e) 0.6 μM, (f) 0.8 μM, (g) 1.0 μM, and (C) the calibration plot for the SWV peak current *vs c*; (E) three-arm DNA junction: (a) 0.05 μM, (b) 0.1 μM, (c) 0.2 μM, (d) 0.4 μM, (e) 0.6 μM, (f) 0.8 μM, (g) 1.0 μM, and (F) the corresponding calibration plot for the SWV peak value *vs c*; (H) four-arm DNA junction: (a) 0.01 μM, (b) 0.05 μM, (c) 0.1 μM, (d) 0.2 μM, (e) 0.4 μM, (f) 0.6 μM, (g) 0.8 μM, (h) 1.0 μM, and (I) the corresponding calibration plot for the SWV peak value *vs c* (*c* represents concentration, error bars, SD, *n*=3).

Conversion Efficiency Comparison of M-CMDJA and CMDJA with Different Concentration of Target in Fluorescence.

Table S4. Conversion Efficiency of M-CMDJA and CMDJA with Different Concentration of Target in Fluorescence. (T = 25 °C, c = 1 μM)

c_1 / M	*Two-arm*		*Three-arm*		*Four-arm*	
	Wild	Mismatched	Wild	Mismatched	Wild	Mismatched
5.00×10^{-7}	1.44×10^{0}	-	-	-	-	-
1.00×10^{-7}	5.96×10^{0}	8.26×10^{0}	7.69×10^{0}	-	-	-
1.00×10^{-8}	5.01×10^{1}	6.74×10^{1}	6.35×10^{1}	8.79×10^{1}	8.08×10^{1}	-
5.00×10^{-9}	-	-	-	-	-	1.92×10^{2}
1.00×10^{-9}	3.88×10^{2}	5.70×10^{2}	5.31×10^{2}	7.27×10^{2}	6.83×10^{2}	7.70×10^{2}
1.00×10^{-10}	2.78×10^{3}	4.33×10^{3}	4.17×10^{3}	6.03×10^{3}	5.54×10^{3}	6.31×10^{3}
1.00×10^{-11}	1.95×10^{4}	3.19×10^{4}	2.98×10^{4}	4.62×10^{4}	4.30×10^{4}	5.01×10^{4}
5.00×10^{-12}	-	4.37×10^{4}	-	-	-	-
1.00×10^{-12}	-	-	1.96×10^{5}	3.56×10^{5}	3.06×10^{5}	3.36×10^{5}
5.00×10^{-13}	-	-	-	5.00×10^{5}	4.15×10^{5}	-
1.00×10^{-13}	-	-	-	-	-	1.96×10^{6}

Conversion Efficiency of M-CMDJA and CMDJA with Different Concentration of Target in Electrochemistry

Table S5. Conversion Efficiency of M-CMDJA and CMDJA with Different Concentration of Target in Electrochemistry (T = 25 °C, c = 1 μM)

c_1 / M	*Two-arm*		*Three-arm*		*Four-arm*	
	Wild	Mismatched	Wild	Mismatched	Wild	Mismatched
1.00×10^{-8}	-	9.09×10^{1}	6.65×10^{1}	9.04×10^{1}	-	-
1.00×10^{-9}	6.14×10^{2}	7.79×10^{2}	5.67×10^{2}	7.58×10^{2}	5.78×10^{2}	8.38×10^{2}
1.00×10^{-10}	5.03×10^{3}	6.44×10^{3}	4.59×10^{3}	5.67×10^{3}	4.99×10^{3}	7.38×10^{3}
1.00×10^{-11}	3.97×10^{4}	5.01×10^{4}	3.43×10^{4}	4.58×10^{4}	4.11×10^{4}	5.97×10^{4}
1.00×10^{-12}	2.92×10^{5}	3.74×10^{5}	2.49×10^{5}	3.35×10^{5}	3.33×10^{5}	4.60×10^{5}
1.00×10^{-13}	1.88×10^{6}	2.02×10^{6}	1.39×10^{6}	1.45×10^{6}	2.24×10^{6}	3.56×10^{6}
5.00×10^{-14}	1.53×10^{6}	-	6.25×10^{5}	-	-	-
2.00×10^{-14}	-	4.75×10^{6}	-	5.93×10^{6}	-	-
1.00×10^{-14}	-	-	-	-	1.38×10^{7}	2.11×10^{7}
1.00×10^{-15}	-	-	-	-	-	1.05×10^{8}
5.00×10^{-16}	-	-	-	-	-	2.26×10^{7}

Optimization of the M-CFDJA in Electrochemical Biosensing Platform Construction

Because the accuracy and the sensitivity of this proposed biosensor largely depend on the efficiency of the M-CFDJA, the reaction time of M-CFDJA and wild CFDJA that influence the efficiency of them were optimized. As the results shown in Fig. S9A, in wild CFDJA, the current response gradually increased with a dilated reaction time from 15 to 90 min, and thereafter reached a plateau, suggesting the reaction equilibrium after 90 min. Impressively, in M-CFDJA, the current response reached a plateau after 30 min which is three times shorter that of CFDJA. Therefore, the reaction time of CFDJA and M-CFDJA in electrochemical biosensor construction was selected at 90 min and 30 min, respectively.

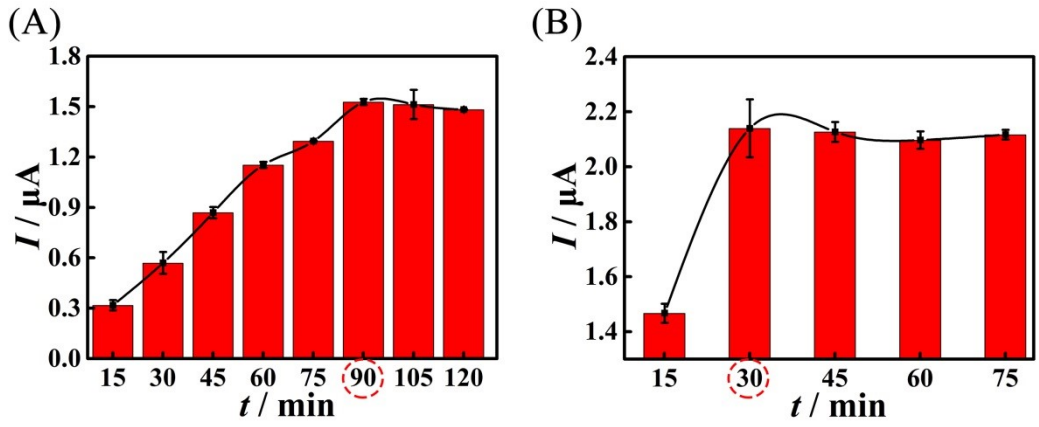

Fig. S9. Effect on the current response of the proposed biosensor with different reaction times of (A) wild CFDJA (15 min, 30 min, 45 min, 60 min, 75 min, 90 min, 105 min, and 120 min) and (B) M-CFDJA with two mismatches (15 min, 30 min, 45 min, 60 min, 75 min, with DNA reactants concentration of 1 μM, miRNA-182-5p concentration of 1 nM, and reaction temperature of 25 °C, Tris-HCl 7.4) (error bars, SD, *n*=3).

Detection Limit Calculation of the Biosensing Platform for the miRNA Biosensing

On the basis of IUPAC definition, we have calculated the limit of detection according to equation (1) and the calibration plot (2) (x_B: the SWV intensity of blank sample, s_B: the standard deviation of blank samples, $k = 3$[5]).

$$I_L = x_B + k \times s_B \quad (1)$$

$$I = 0.3016 \lg c + 5.3702 \quad (2)$$

In this work, the SWV measurements for blank samples (M-CFDJA) were carried out with ten parallel tests, showing an x_B of 0.15 μA and a s_B of 1.08×10^{-8} μA. The electrochemical signal intensity of detection limit (I_L) is therefore calculated to be 0.18 μA. Based on the equation of the calibration (2), the detection limit is computed to be 6.11 aM. Similarly, the detection limit of biosensing platform based on other CMDJA and M-CMDJA for miRNA-182-5P detection were also calculated (Table S6).

Table S6. Detection Limit Calculation of the Biosensor for the miRNA Biosensing (n=10)

Electrochemical Biosensors	x_B	s_B	I_L	LOD
CTDJA (two arm) / μA	0.10	0.022	0.17	2.6 fM
M-CTDJA (two arm) / μA	0.15	0.026	0.23	0.95 fM
CTDJA (three arm) / μA	0.088	0.013	0.13	4.6 fM
M-CTDJA (three arm) / μA	0.16	0.0094	0.19	1.3 fM
CFDJA (four arm) / μA	0.062	0.0076	0.084	0.54 fM
M-CFDJA (four arm) / μA	0.15	0.011	0.18	6.11 aM

Performance Evaluation of the Electrochemical Biosensor

In order to evaluate the performance of the developed biosensor based on M-CFDJA, we investigated the essential indexes for a real biomarker detection

containing reproducibility, selectivity and stability of the biosensor. To study the reproducibility of the biosensor, the electrochemical signal response of four assembled biosensors with 10 pM miRNA-182-5p were monitored. As the results exhibited in Fig.S10A, a relative standard deviation (RSD) of 6.31% was realized. Otherwise, after 15 days, another four prepared biosensors with same miRNA-182-5P (10 pM) were detected with a RSD of 5.05%. The results further suggest that the use of the high-efficiency M-CFDJA endowed the biosensor with a desirable reproducibility.

For studying the selectivity of the biosensing platform, three interference agents containing miRNA-21, miRNA-141, and miRNA-155 were assessed by SWV measurements. As displayed in Fig. S10B, only in the presence of the miRNA-182-5P (10 pM, e), evident electrochemical signal response of the electrode could be noticed. Oppositely, when the interference agents including miRNA-21 (1 nM, b), miRNA-141 (1 nM, c), and miRNA-155 (1 nM, d) participate the reaction of biosensing process, the electrochemical signal were nearly unconspicuous. Besides, the mixed sample containing 10 pM of target miRNA-182-5p was also detected, showing an electrochemical signal response as expected (f). The results above suggested the high selectivity of the biosensing platform.

The stability was investigated by storing the prepared sensing platform at 4 °C and measuring per 3 days. As the results shown in Fig. S10C, in comparison with the initial current response of the sensing platform, the electrochemical signal intensity just varied from 100.00 % to 94.50% (RSD=2.53%), verifying an acceptable stability

of our sensing platform.

The capacity of the proposed biosensor for determination of miRNA-182-5p in real biological samples was also evaluated by obtaining the total RNA extraction solutions from the human cancer cell lines (22RV1, A549, and HeLa). As shown in Fig. S10D, the SWV current response increased as the elevated number of cells, displaying an obvious expression level of target miRNA-182-5P from 22RV1 and A549, whereas in blank sample and HeLa cells, no obvious SWV responses were noticed, indicating a quite lower expression level compared with those of 22RV1 and A549 cells. The above results were in accordance with previous research,[6,7] further suggesting this biosensing platform based on M-CFDJA for miRNA-182-5p detection in cancer cells has the great potential in the area of clinical cancers diagnosis.

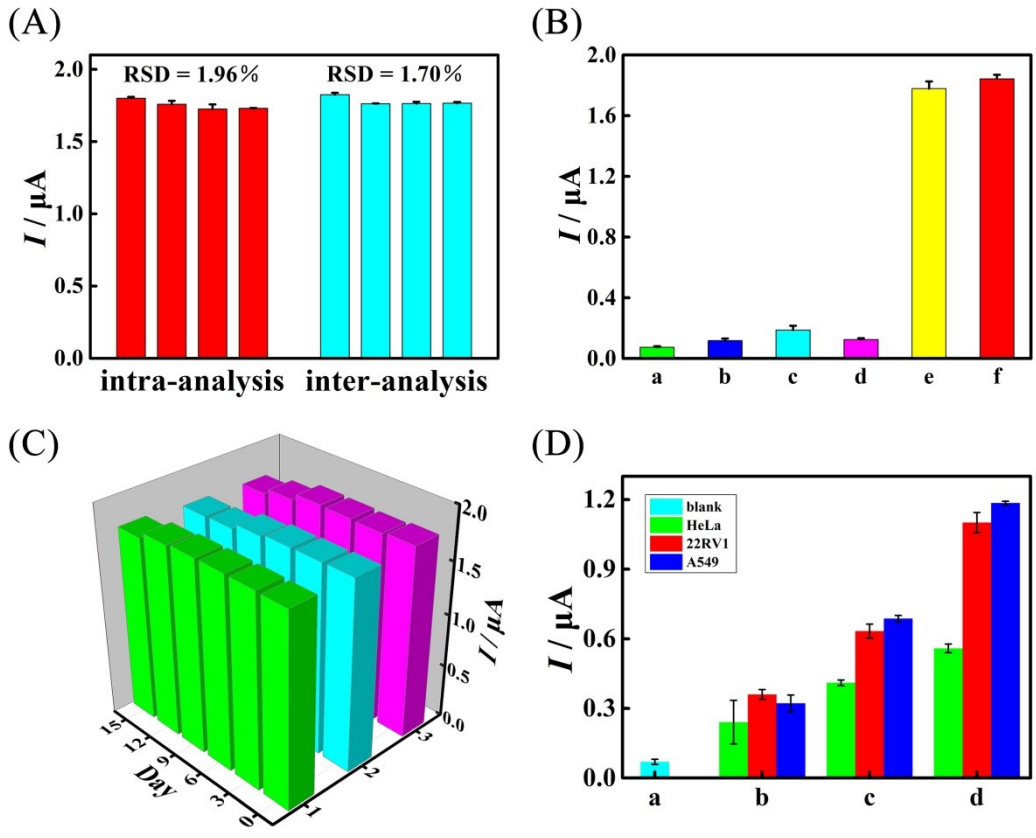

Fig. S10. (A) The reproducibility (10 pM miRNA-182-5p) of sensing platform, (B) the selectivity

of the sensing platform: (a) blank sample, (b) miRNA-21 (1 nM), (c) miRNA-141 (1 nM), (d) miRNA-155 (1 nM), (e) miRNA-182-5p (10 pM), and (f) mixed sample, and (C) the stability of the prepared sensing platform (10 pM miRNA-182-5p, n=3). (D) Data analysis of the proposed sensing platform with different cancer-cell lysates: (a) Blank sample, (b) HeLa (100 cells), 22RV1 (100 cells), and A549 (100 cells), (c) HeLa (1000 cells), 22RV1 (1000 cells), and A549 (1000 cells), and (d) HeLa (10000 cells), 22RV1 (10000 cells), and A549 (10000 cells) (Error bars, SD, n = 3).

References

1 F. Wang, C. Ye, S. Mo, H. Luo, J. Chen, Y. Shi, N. Li. Enhanced photoelectrochemical sensing based on novel synthesized Bi_2S_3@Bi_2O_3 nanosheet heterostructure for ultrasensitive determination of L-cysteine. *Anal. Bional. Chem.*, 2019, **411**, 3059-3068.

2 X. L. Zhang, Y. Yin, S. M. Du, L. Q. Kong, Z. H. Yang, Y. Y. Chang, Y. Q. Chai, R. Yuan. Programmable high-speed and hyper-efficiency DNA signal magnifier. *Adv. Sci.*, 2022, **9**, 2104084.

3 X. L. Zhang, Z. H. Yang, Y. Y. Chang, D. Liu, Y. R. Li, Y. Q. Chai, Y. Zhuo, R. Yuan. Programmable mismatch-fueled high-efficiency DNA signal converter. *Chem. Sci*., 2020, **11**, 148-153.

4 J. Zhang, S. Song, L. Wang, D. Pan, C. Fan. Photochemical synthesis of electrically conductive CdS nanowires on DNA scaffolds. *Nat*. *Protoc*., 2007, **2**, 2888-2895.

5 P. Zhang, J. Jiang, R. Yuan, Y. Zhuo, Y. Q. Chai. Highly ordered and field-free 3D DNA nanostructure: The next generation of DNA nanomachine for rapid single-step sensing. *J. Am. Chem. Soc.*, 2018, **140**, 9361-9364.

6 L. Yang, Y. Dou, Z. X. Sui, H. Cheng, X. Liu, Q. L. Wang, P. F. Gao, Y. Qu, M. Xu. Upregulated miRNA-182-5p expression in tumor tissue and peripheral blood samples from patients with non-small cell lung cancer is associated with downregulated Caspase 2 expression. *Exp. Ther. Med.*, 2020, **19**, 603-610.

7 C. H. Gu, K. Y. Zhao, N. C. Zhou, F. Liu, F. Xie, S. L. Yu, Y. J. Feng, L. Chen, J. J. Yang, F. Y. Tian, G. S. Jiang. UBAC2 promotes bladder cancer proliferation through

BCRC-3/miRNA-182-5p/p27 axis. *Cell. Death. Dis.*, 2020, **11**, 733.